Transfer of CVD-grown graphene for room temperature gas sensors

F. Rigoni[1,2], R. Maiti[1], C. Baratto[2,1], M. Donarelli[1,2], J. MacLeod[3], B. Gupta[3], M. Lyu[3], A. Ponzoni[2,1], G. Sberveglieri[4], N. Motta[3] and G. Faglia[1,2]

[1]*Sensor Lab, Department of Information Engineering, University of Brescia, Via Branze 38, 25123 Brescia, Italy*

[2]*Sensor Lab. CNR-INO Via Branze 45, 25123 Brescia, Italy*

[3]*School of Chemistry, Physics and Mechanical Engineering, Queensland University of Technology (QUT), 2 George Street, Brisbane 4001 Queensland, Australia*

[4]*Nano Sensor Systems srl, University of Brescia, Via Branze 38, 25123 Brescia, Italy*

Abstract

An easy transfer procedure to obtain graphene-based gas sensing devices operating at room temperature is presented. Starting from chemical vapor deposition (CVD)-grown graphene on copper foil, we obtained single layer graphene which could be transferred onto arbitrary substrates. In particular, we placed single layer graphene on top of a SiO_2/Si substrate with pre-patterned Pt electrodes to realize a chemiresistor gas sensor able to operate at room temperature. The responses to ammonia (10, 20, 30 ppm) and nitrogen dioxide (1, 2, 3 ppm) are shown at different values of relative humidity, in dark and under 254 nm UV light. In order to check the sensor selectivity, gas response has also been tested towards hydrogen, ethanol, acetone and carbon oxide. Finally, a model based on linear dispersion relation characteristic of graphene, which take into account humidity and UV light effects, has been proposed.

1. Introduction

Gas sensors play a relevant role in our daily life in increasingly wider fields of application, e.g. environmental monitoring [1, 2], medical diagnosis [3, 4], industrial safety [5], security and food quality fields [6]. Over the past several decades, tremendous development has been observed in the field of chemical sensors, mostly based on semiconducting metal oxides [7]. The advantage of those solid state gas sensors are their small size, low power consumption, high sensitivity, low cost and versatility, which allows the detection of a wide range of target gases at very low concentrations (of the order of ppm and for very reactive gases ppb). The performance of these devices is still limited due to drawbacks regarding their lack of long term stability, poor selectivity and typical operation at high working temperatures. Hence, the aim is to obtain the next generation of sensor devices, working at room temperature (RT) with low power consumption and enhanced sensing performances such as ultrahigh sensitivity at low concentrations, fast response and recovery times.

In recent decades, nanostructured allotropes of carbon have begun to be used as solid state gas sensors (in particular carbon nanotubes [8] and graphene [9]). After its discovery in 2004 [10], graphene has created lot of buzz among the scientific communities due to its fascinating physical properties. Graphene is the 2-D analogue of graphite, one atom thick, with a large specific surface area, low electrical noise and exceptionally high carrier mobility (up to 2×10^5 $cm^2V^{-1}cm^{-1}$) at RT, making it an ideal platform for the fabrication of ultrasensitive and ultrafast sensors [9, 11]. The possibility to operate at RT is one of the main objectives of using graphene as active material for gas sensing, instead of metal-oxide-based devices, which usually require high operating temperatures. The first experiment reported on the detection of gas molecules based on graphene was carried out in 2007 by Schedin et al. [12]. After this, a wide range of chemicals, biomolecules and gas/vapors has been detected using graphene-based sensors [13-24].

Here, we report the transfer mechanism of a CVD-grown graphene on Cu foil onto a pre-patterned SiO_2/Si substrate, in order to fabricate RT gas sensor devices.

RT sensing behaviors of these devices in presence of oxidizing and reducing target gases (NO_2 and NH_3, respectively) in various relative humidity (RH) environments, under both the illumination of 254 nm UV light and in dark conditions, are reported. Electron acceptors such as NO_2 and electron donors such as NH_3 can be detected by observing their effects on the conductivity of the graphene. Electron acceptors increase the hole concentration, which leads to a conductivity increase, whereas electron donors compensate the hole concentration, leading to a decrease of the conductivity: these behaviors are a fingerprint of the p-type conductivity of the transferred graphene. Response to UV light has been studied both in air and in inert atmosphere (Ar), showing that the UV main effect is to remove the adsorbed species on top of the graphene layer. During gas exposures, UV light improves the relative response to gases and the recovery of the signal after gas exposure, which is slow at RT.

2. Experimental

2.1 Transfer procedure of CVD-grown graphene from Cu foil onto SiO_2 substrate

Starting from Refs. [25, 26], a wet chemical approach has been followed in order to transfer the CVD-grown monolayer graphene from a copper foil (Graphene Supermarket) onto any arbitrary substrate. Three different substrates were used and Raman characterization has been carried out (data are shown in Fig. S1 of the Supplementary Information). Hereafter, our attention will be focused on the graphene transfer onto SiO_2/Si substrate with pre-patterned electrodes deposited by Electron Beam Lithography (EBL). Briefly, in this process, a 550 nm thick polymethyl methacrylate (PMMA) layer was deposited by spin coating on a 100 nm SiO_2/Si substrate and subsequent annealing has been done at 180 °C. The electron beam, controlled by external software, directly patterned the PMMA layer. Then, the substrate was rinsed in a methyl isobutyl ketone (MIBK) and isopropanol solution (MIBK:IPA, 1:3) for 90 s and in isopropanol for 2 min. After that, the PMMA exposed areas have been removed, and about 20 nm of Ti-W (adhesive layer) and 350 nm of Pt were deposited on the sample by magnetron sputtering. After rinsing in acetone, the unexposed areas of PMMA were also removed, leaving only the patterned electrodes on the surface.

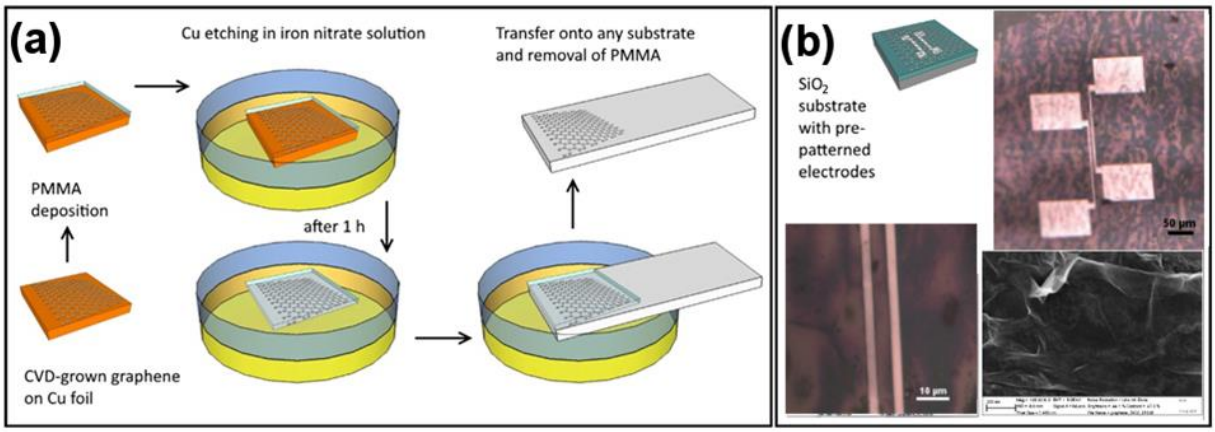

Fig. 1. Panel (a): scheme of the transfer of CVD-grown graphene from copper foil to any substrate. Panel (b): clockwise: sketch of the transferred and deposited graphene on prepatterned substrates; optical microscope image of the device, with Pt electrodes and graphene on them; SEM image of the graphene layer; zoom-in of the electrodes (optical microscope image).

As graphically described in Fig.1, panel (a), the following transfer procedure steps have been adopted: (1) starting from monolayer CVD-grown graphene on copper foil (Graphene Supermarket), a film of PMMA has been deposited by spin coating (5 µL of PMMA in chloroform, spin coated on graphene/Cu at 1000 rpm for 5 s, 4000 rpm for 5 s, 6000 rpm for 30 s); (2) 12 hours drying at RT; (3) backside etching of the copper foil by O_2 plasma (100 W, 180 s, O_2 concentration 30%) in order to remove graphene from the back; (4) copper etching in iron nitrate solution (after the copper etching process, the stack of PMMA/graphene floats on the solution surface); (5) rinsing in DI water and Standard Cleaning (SC: 15 min in acetone, 15 min in isopropanol)

procedures: DI rinse, SC-2, DI rinse, SC-3, DI rinse; (6) baking at 150 °C for 15 min; (7) PMMA removal (acetone and IPA rinse); (8) baking at 200 °C for 15 min. In Fig. 1, panel (b), the prepatterned electrodes are depicted. The spacing between two electrodes is about 10 µm. The fabricated device is then analyzed by Scanning Electron Microscopy (FE-SEM, Zeiss LEO 1525) and optical microscopy.

2.2 Raman and gas sensing set-up

The quality of the graphene layer after the transfer procedure has been verified by Raman spectroscopy. Raman spectra of graphene after the transfer onto different substrates were obtained using a micro-Raman spectrometer (inVia Renishaw) with 532 nm laser excitation source (Fig.2 panel (a) and Fig. S1 of the Supplementary Information). Raman spectra were carried out to probe the change in quality before and after the gas sensing measurements with a Horiba modular micro-Raman system using a 100x objective at the same excitation wavelength (532 nm).

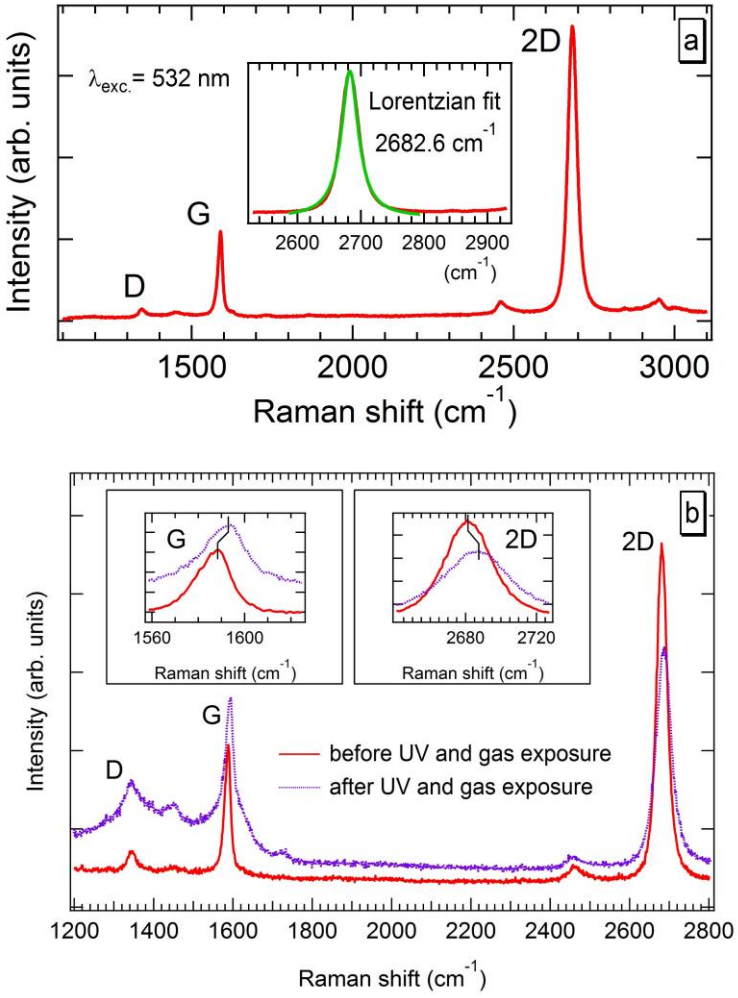

Fig. 2. Panel (a): Raman spectrum of the graphene transferred on top of SiO_2 substrate. The background due to the substrate has been subtracted. Insets: the 2D band (red curve) and its fitting curve (Lorentzian curve centered at (2682.60 ± 0.05) cm^{-1}). Panel (b): Raman spectra of graphene on SiO_2 substrate, before (red curve) and after UV and gas exposures (violet curve). After UV and gas exposure, the 2D band is broadened and shifted at (2686.10 ± 0.08) cm^{-1}.

Gas sensing measurements were carried out in a gas testing chamber (1 L volume) equipped with two gas lines, mass flow controllers and an optical quartz window. The system dynamically reproduces environmental conditions in a controlled and repeatable way and it is based on volumetric mixing through mass flow controllers and certified bottles. Oxidizing gases, e.g. nitrogen dioxide, and reducing gases like ammonia,

ethanol and acetone diluted in dry and humid air at 30% RH were tested. The total flow during the measurements was 300 cm^3/min. The gas sensing measurements were performed at atmospheric pressure, in dry air and with 30% RH, at RT (20 °C). A constant bias (0.01 V) was applied to the sensing layer and the electrical current was measured by a picoammeter (Keithley, model 486).

3. Results and discussion

3.1 Raman characterization

The properties of graphene are very much dependent on the production method and disorder strongly affects them [27]. Raman characterization has been carried out in order to check the quality of the graphene layer after the transfer procedure and to probe the disorder of the graphene deposited onto the different substrates (see Fig. S1 of the Supplementary Information). Raman spectra of graphene deposited onto SiO_2 substrate device have been taken before and after gas sensing measurements (i.e. after exposing the graphene layer to reducing and oxidizing gases, and under UV irradiation).

Fig. 2 shows the typical Raman spectra of graphene transferred onto SiO_2/Si substrate with the typical D, G and the 2D spectral features respectively centered at 1344 cm^{-1}, 1589 cm^{-1} and 2683 cm^{-1}. The D peak is the so-called "defect-related" peak because it is activated by defects that induce breathing modes of the sp^2 atoms. The G peak is related to the E_{2g} phonon of graphene, whereas the second order of D, the 2D peak, originates due to the second order phonon [28]. In the insets of Fig. 2, panel (a), the 2D band (red curve) fitted with a Lorentzian curve (green curve) centered at (2682.60 ± 0.05) cm^{-1} is shown. The number of layers can be obtained from the 2D peak shape and position [29]. The analysis of the 2D peak allows us to conclude that the transferred graphene sheet is monolayer.

Fig. 2, panel (b), shows the Raman spectra of graphene on SiO_2/Si substrate before (red curve) and after (violet curve) gas sensing measurements and UV irradiation. After UV and gas exposures, we observed a pronounced increase of the D peak intensity, a shift of the G band (from 1588.4 cm^{-1} to 1593.8 cm^{-1}) and a shift (from 2683 cm^{-1} to 2686.1 cm^{-1}) and broadening of the 2D band, as expected for UV-damaged and disordered graphene [27]. The intensity increase of the defect related peak, the G and 2D shifts and the 2D broadening are attributed more to the UV irradiation than to the few ppm target gas exposure. In accordance with literature [27, 30, 31], we observed that the exposure to UV light might increase the number of defects on the graphene layer.

3.2 UV effect

The main change induced by UV (λ = 254 nm) light irradiation is the increase of the electrical resistance of the graphene-based devices. Fig. 3 shows the dynamical response to UV in two different atmospheric conditions: under synthetic air (Fig. 3, panels (a) and (b)) and Ar flow (Fig. 3, panels (c) and (d)). In Fig. 3, panels (b) and (d), we analyzed the rise time and the recovery time, using double-exponential functions:

$$y=y_0+A\exp[(x-x_0)/\tau_1]+B\exp[(x-x_0)/\tau_2],$$

where τ_1 and τ_2 are the two characteristic time constants.

In Table 1, the estimated values of τ_1 and τ_2 are reported.

Calculated from double exp. fit	Synthetic air	Ar atmosphere
τ_1 (rise)	(0.760 ± 0.005) min	(1.71 ± 0.02) min
τ_2 (rise)	(3.15 ± 0.03) min	(15.0 ± 0.1) min
τ_1 (recovery)	(2.77 ± 0.03) min	(4.70 ± 0.05) min
τ_1 (recovery)	(34.6 ± 0.3) min	(50.4 ± 0.6) min

Table 1. τ_1 and τ_2 calculated values from the double-exponential function used to analyze the rise and recovery times.

The resistance variation in Ar atmosphere is greater than in synthetic air during UV exposure. The response to UV in synthetic air shows a very fast rise time, reaching a quasi-saturation regime after 20 min UV irradiation and the recovery dynamic is much faster with respect to the UV exposure in Ar atmosphere. These observations could be explained by considering that UV light induces the desorption of oxygen species from the graphene surface. Like carbon nanotubes [32], graphene also exhibits p-type nature in standard ambient conditions, due to the presence of atmospheric oxygen [33]: the negative charges transferred to the electron trapping adsorbate group O_2^- lead to an increase of holes in the graphene valence band, making graphene a p-type semiconductor. This process is defined by the following adsorption half-reaction:

O_2 (g) + e^- → O_2^- (ads)

The electron-hole pair generation upon UV exposure promotes the desorption of oxygen adsorbates via hole recombination [34], described by the desorption reaction:

$h^+ + O_2^-$ (ads) → O_2 (g)

The resistance increase results from a decrease in the hole concentration, which is due to the recombination of holes with O_2^-. If we consider that graphene is p-type doped (by O_2^- molecule adsorbed on top of the graphene surface at room temperature, with one extra hole in the valence band) and that one electron-hole couple is generated by the UV irradiation, the hole (of electron-hole pair) recombines with the O_2^- that desorbs from the surface and the electron recombines with the extra hole in the valence band. The net effect is that there is one hole less in the valence band. This is consistent with the resistance increase experimentally observed.

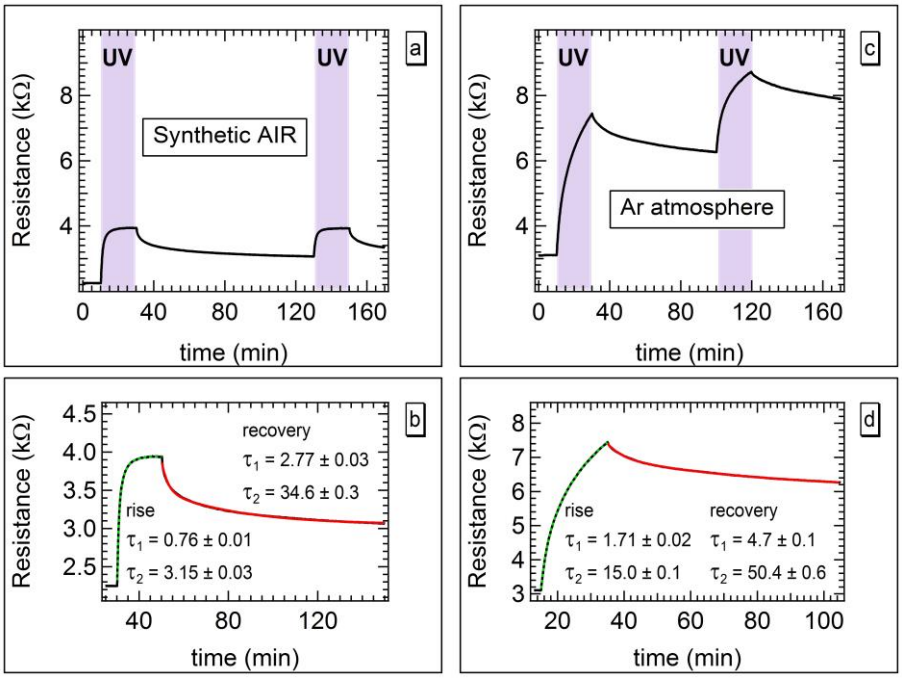

Fig. 3. UV light (λ = 254 nm) effect on graphene sample in two different atmospheres: synthetic dry air (top left) and inert Ar atmosphere (top right). Bottom: resistance of the device when the UV is switched on ("rise") and after the UV is switched off ("recovery") in synthetic dry air (left) and in inert Ar atmosphere (right). The green (red) curves represent the fitting curves of the resistance vs. time after UV is switched on (off). The related time constants of the double exponential fitting functions are reported in the graphs.

3.3 Gas response to NO_2 and NH_3

The gas sensing responses to NO_2 and NH_3 at RT of the graphene-based device examined in dark and under UV exposure, and at two different RH values, are reported in Fig. 4. We observe a resistance decrease when

exposed to oxidizing gases like NO_2, and a resistance increase upon exposure to reducing gases like NH_3, confirming the p-type nature of the sensing material. In dark conditions, a very low variation of the electrical resistance during gas exposures takes place (black dashed curves in Fig. 4). UV light (λ = 254 nm) irradiation enhances the response towards both the oxidizing and reducing gases (blue solid lines in Fig. 4, panels (a) and (b)).

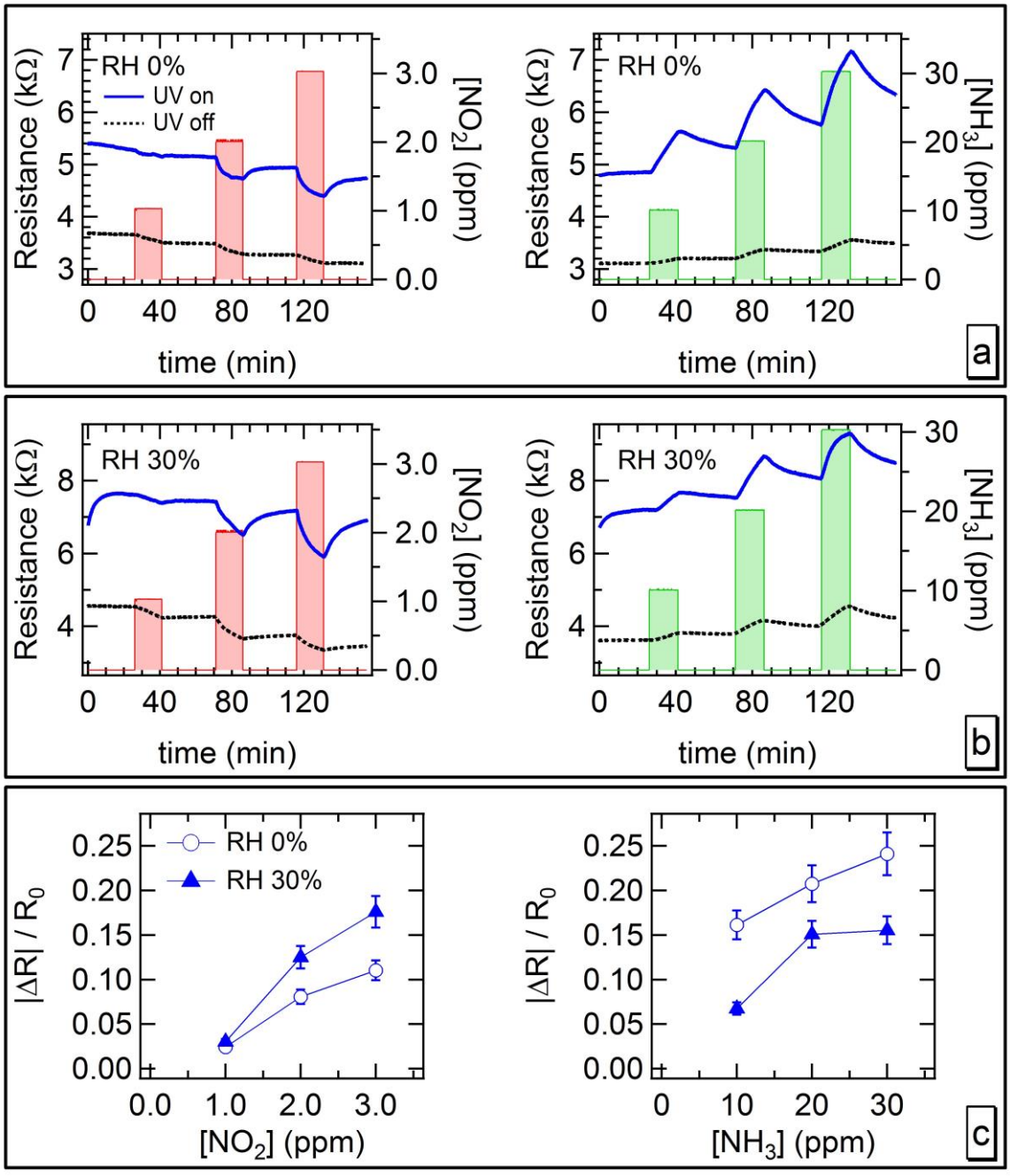

Fig. 4. Electrical gas responses of graphene-based device in dark condition (black dashed curve) and under UV irradiation (blue solid curve) to NO_2 (left graphs) and NH_3 (right graphs) at two different level of relative humidity, namely 0% (panel a) and 30% (panel b). Panel (c): relative responses to NO_2 (left) and NH_3 (right) of the UV illuminated sample at the two different levels of RH. Temperature is kept constant at 20°C. The heights of the red (green) rectangles represent the concentrations of NO_2 (NH_3).

The improved gas sensing responses of the UV-exposed graphene layer could be ascribed to both the UV effects previously discussed: (1) the increased number of defects and (2) the desorption of oxygen from the surface, which leads to an increased number of free available sites for the target gases. UV radiation allows

also a relatively quick recovery after NO_2 gas exposure, while after NH_3 exposure the recovery time is much longer. Fig. 4, panel (c) shows the relative response to NO_2 (left) and NH_3 (right) of the UV illuminated sample at the two different levels of RH (0% and 30%). The sample displays an enhanced response to NO_2 with RH=30% and to NH_3 in dry air. We can explain this effect by considering the role of H_2O interaction with the graphene layer.

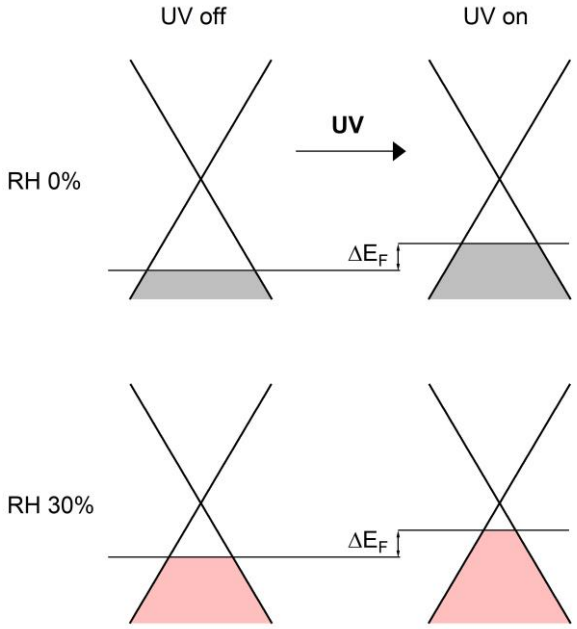

Fig.5. Schematic view of the linear dispersion relation characteristic of graphene in dry air (top) and in 30% RH (bottom) atmospheres. H_2O reducing molecules adsorbed on top of graphene inject extra electrons in the valence band shifting the Fermi level upward. The UV effect is seen from left (UV off) to right (UV on). UV light induces desorption of negatively charged oxygen species from the graphene surface and shifts the Fermi level further upward.

Although many works in literature report on the acceptor nature of H_2O molecule when it is adsorbed on the graphene surface [12, 14, 35, 36, 37], the real effect of humidity on the electrical properties of graphene is still controversial. For example, some researchers observe reducing behavior due to H_2O adsorption. Zheng et al. [38] demonstrate that pre-treatment with H_2O can induce n-type doping of graphene. Other works show the electrical response to humidity: by increasing RH, the resistance increase, due to the negative charge injected by the reducing H_2O to p-type graphene [39, 40], and p-type graphene oxide [41], or increasing graphene oxide resistance passing from dry to humid atmosphere [42].

From the presently reported gas sensing tests, we can summarize that: (i) increasing RH leads to resistance increase (Fig. S2, Supplementary Information); (ii) the graphene-based device shows a better relative response to NO_2 in humid atmosphere (RH = 30%) than in dry air (Fig. 4, panel (c), left); (iii) the graphene-based device shows a better relative response to NH_3 in dry air than in humid atmosphere (RH = 30%) (Fig. 4, panel (c), right).

The UV and RH effects can be explained by a model based on the band structure of graphene, as shown schematically in Fig. 5. Water molecules adsorbed on top of graphene inject extra electrons in the valence band. This causes an upward shift of the Fermi level (as sketched in Fig. 5, “UV off”, the Fermi level at RH 30% is above the one related to RH 0%). UV light induces the desorption of negatively charged oxygen species from graphene, releasing trapped electrons. This leads to a further upward shift of the Fermi level (Fig. 5, from “UV off” to “UV on”). This rationale can justify the opposite effects of humidity on the relative responses toward NO_2 and NH_3, reported in Fig. 4, panel (c). At RH = 30%, H_2O reducing molecules inject extra electrons into the graphene, promoting the interaction between graphene and the NO_2 oxidizing molecules. On the other

hand, regarding NH_3 sensing, the injected extra electrons disadvantage the interaction between ammonia-reducing molecules and graphene. The same behavior, i.e. better response in dry air than with RH=30%, has been observed for other reducing gases like ethanol, acetone, H_2 and CO (some data reported in the Supplementary Information). However, although enhanced by UV irradiation, the response towards very high concentrations of these gases is still negligible.

4. Conclusions

We have transferred CVD-grown monolayer graphene from copper foil onto arbitrary substrates, by following a PMMA assisted wet chemical procedure. Raman characterization has been carried out in order to check the quality of the transferred graphene onto three different substrates: glass, Si and SiO_2/Si. Graphene-based gas sensing devices have been fabricated by transferring a graphene sheet on top of pre-patterned SiO_2/Si substrates. The graphene-based device increases its resistance under UV illumination. RT gas sensing responses to NO_2, NH_3, H_2 and ethanol, enhanced under UV light, have been reported. The illuminated device shows better sensing performance in humid atmosphere, in the case of NO_2 detection, and in dry air, in the case of NH_3 sensing. The effects of humidity and UV exposure on the gas sensing performances and electrical properties of the graphene are consistent with a simple model based on Fermi level shifting due to doping. The reported results are promising for the development of graphene based gas sensors, with low-ppm sensitivity to NO_2 and NH_3, working at RT.

Acknowledgements

The research leading to these results were partially funded by the NATO Science for Peace and Security Programme under grant N° 9085043. The authors would like to acknowledge QUT Central Analytical Research Facility and Queensland Chinese Academy of Science Collaboration Fund on Graphene Thin Film Supercapacitors.

References

[1] Fine GF, Cavanagh LM, Afonja A, Binions R 2010 Sensors **10** 5469-5502
[2] Timmer B, Olthuis W, van den Berg A 2005 Sensors and Actuators B **107** 666–677
[3] Ryabtsev SV, Shaposhnick AV, Lukin AN, Domashevskaya EP 1999 Sensors and Actuators B **59** 26-29
[4] Righettoni M, Tricoli A, Pratsinis SE 2010 Anal. Chem. **82** 3581-3587
[5] Liu X, Cheng S, Liu H, Hu S, Zhang D, Ning H 2012 Sensors **12** 9635-9665
[6] Ponzoni A, Comini E, Concina I, Ferroni M, Falasconi M, Gobbi E, Sberveglieri V, Sberveglieri G 2012 Sensors **12** 17023-17045
[7] Comini E, Faglia G, Sberveglieri G 2009 Solid State Gas Sensing Springer
[8] Zhang T, Mubeen S, Myung NV, Deshusses MA 2008 Nanotechnology **19** 332001
[9] Varghese SS, Lonkar S, Singh KK, Swaminathan S, Abdala A 2015 Sensors and Actuators B **218** 160
[10] Novoselov KS, Geim AK, Morozov SV, Jiang D, Zhang Y, Dubonos SV, Grigorieva IV, Firsov AA 2004 Science **306** 666
[11] Meng F-L, Guo Z, Huang X-J 2015 Trends in Analytical Chemistry **68** 37
[12] Schedin F, Geim AK, Morozov SV, Hill EW, Blake P, Katsnelson MI, Novoselov KS 2007 nature materials **6** 652-655
[13] Wehling TO, Novoselov KS, Morozov SV, Vdovin EE, Katsnelson MI, Geim AK, Lichtenstein AI 2007 Nano Lett. **8** 173
[14] Leenaerts O, Partoens B, Peeters FM 2008 Phys. Rev. B **77** 125416
[15] Huang B, Li Z, Liu Z, Zhou G, Hao S, Wu J, Gu B-L, Duan W 2008 J. Phys. Chem. C **112** 13442
[16] Robinson JT, Perkins FK, Snow ES, Wei Z, Sheehan PE 2008 Nano Lett. **8** 3137

[17] Dan Y, Lu Y, Kybert NJ, Luo Z, Johnson ATC 2009 Nano Lett. **9** 1472
[18] Fowler JD, Allen MJ, Tung VC, Yang Y, Kaner RB, Weiller BH 2009 ACS Nano **3** 301
[19] Dua V, Surwade SP, Ammu S, Agnihotra SR, Jain S, Roberts KE, Park S, Ruoff RS, Manohar SK 2010 Angew. Chem. **49** 2154
[20] Johnson JL, Behnam A, An Y, Pearton SJ, Ural A 2011 J. Appl. Phys. **109** 124301
[21] Yavari F, Chen Z, Thomas AV, Ren W, Cheng H-M, Koratkar N 2011 Sci. Rep. **1** 166
[22] Gautam M, Jayatissa AH 2012 J. Appl. Phys. **111** 094317
[23] Tsetseris L, Pantelides ST 2012 Phys. Rev. B **85** 155446
[24] Yuan W, Liu A, Huang L, Li C, Shi G 2013 Adv. Mater. **25** 766
[25] Liang X, Sperling BA, Calizo I, Cheng G, Hacker CA, Zhang Q, Obeng Y, Yan K, Peng H, Li Q, Zhu X, Yuan H, Walker AR, Liu Z, Peng LM, Richter CA 2011 ACS Nano **5** 9144-9153
[26] Li X, Zhu Y, Cai W, Borysiak M, Han B, Chen D, Piner RD, Colombo L, Ruoff RS 2009 Nano Lett. **9** 4359-4363
[27] Casiraghi C 2009 Phys. Status Solidi RRL **3** 175–177
[28] Thomsen C, Reich S 2000 Phys. Rev. Lett. **85** 5214
[29] Ferrari AC, Meyer JC, Scardaci V, Casiraghi C, Lazzeri M, Mauri F, Piscanec S, Jiang D, Novoselov KS, Roth S Geim AK 2006 Phys. Rev. Lett. **97** 187401
[30] Liu H, Ryu S, Chen Z, Steigerwald ML, Nuckolls C, Brus LE 2009 J. AM. CHEM. SOC. **131** 17099-17101
[31] Imamura G, Saiki Koichiro 2013 Chemical Physics Letters **587** 56-60
[32] Collins PG, Bradley K, Ishigami M, Zettl A 2000 Science **287** 1801-1804
[33] Ryu S, Liu L, Berciaud S, Yu Y-J, Liu H, Kim P, Flynn GW, Brus LE 2010 Nano Lett. **10** 4944-4951
[34] Luo Z, Pinto NJ, Davila Y, Johnson ATC 2012 Applied Physics Letters **100** 253108
[35] Maiti UN, Lee WJ, Lee JM, Oh Y, Kim JY, Kim JE, Shim J, Han TH, Kim SO 2014 Adv. Mater. **26** 40-67
[36] Wehling TO, Katsnelson MI, Lichtenstein AI 2008 Appl. Phys. Lett. **93** 202110
[37] Kong L, Enders A, Rahman TS, Dowben PA 2014 J. Phys.: Condens. Matter **26** 443001
[38] Zheng L, Cheng X, Wang Z, Xia C, Cao D, Shen L, Wang Q, Yu Y, Shen D 2015 J. Phys. Chem. C **119** 5995-6000
[39] Randeniya LK, Shi H, Barnard AS, Fang J, Martin PJ, Ostrikov K 2013 Small **9** 3993-3999
[40] Jung I, Dikin D, Park S, Weiwei C, Mielke SL, Ruoff RS 2008 J. Phys. Chem. C **112** 20264-20268
[41] Prezioso S, Perrozzi F, Giancaterini L, Cantalini C, Treossi E, Palermo V, Nardone M, Santucci S, Ottaviano L 2013 J. Phys. Chem. C **117** 10683-10690
[42] Donarelli M, Prezioso S, Perrozzi F, Giancaterini L, Cantalini C, Treossi E, Palermo V, Santucci S, Ottaviano L 2015 2D Materials **2** 0350168